Advances in Science and Technology Research Journal

Advances in Science and Technology Research Journal, 2025, 19(9), 410–427
https://doi.org/10.12913/22998624/207875
ISSN 2299-8624, License CC-BY 4.0

Received: 2025.06.18
Accepted: 2025.07.15
Published: 2025.08.01

The influence of polymer materials and internal density on the parameters of fused filament fabrication samples during tensile testing

Małgorzata Gontarz-Kulisiewicz[1*], Grzegorz Budzik[1], Tomasz Dziubek[1], Bartłomiej Sobolewski[1], Łukasz Przeszłowski[1]

[1] Faculty of Mechanical Engineering and Aeronautics, Rzeszów University of Technology, Al. Powstańców Warszawy 12, 35-959 Rzeszów, Poland
* Corresponding author's e-mail: m.gontarz@prz.edu.pl

ABSTRACT

This article presents a strength analysis of selected polymer materials ABS (acrylonitrile butadiene styrene), PLA (polylactic acid), HABS (hard acrylonitrile butadiene styrene), HIPS (high-impact polystyrene), PC/ABS (acrylonitrile butadiene styrene with polycarbonate), and S&S (strong and soft)) used in the FFF method based on a static tensile test. Standardized type 1A specimens with varying filling densities of the internal grid structure were tested, specifically at densities of 13%, 15%, 20%, 65%, 80%, and fully filled. Additionally, the fractures of the samples following the strength tests were examined and described.

Keywords: FFF method, static tensile test, internal structure, internal infill, ABS, PLA, 3D printing.

INTRODUCTION

Additive manufacturing (AM) is rapidly advancing, largely due to the increasing availability of prototyping devices and the materials used in this process. AM technologies are considered among the most significant in the industry due to their numerous advantages, particularly in the prototyping of components and creating customized products with unconventional geometries that are challenging to produce using traditional methods [1]. Consequently, alongside basic polymer materials, there is a growing marketplace for composite materials that offer enhanced strength properties [2]. When designing components, the assumption of full density in the internal structure is often made to ensure optimal strength under applied loads. However, the actual impact of this density on the strength parameters of the designed machine elements is sometimes overlooked. Additive technologies can significantly reduce material waste and decrease costs related to the finishing of produced models [3].

Among additive manufacturing processes, the most commonly used are stereolithography (SLA), material extrusion (MEX), and selective laser melting (SLM) [1, 4]. Research frequently addresses the strength of models produced using MEX methods, particularly fused filament fabrication (FFF). This focus is due to the accessibility of materials and devices, the compact size of the machines, their lower cost compared to conventional tools, and their ease of use [5, 6]. In the FFF method, a variety of polymer-based composites and thermoplastic materials are used, including ABS (acrylonitrile butadiene styrene), ASA (acrylonitrile styrene acrylate), PEEK (polyetheretherketone), PLA (polylactic acid), PC (polycarbonate), and PETG (polyethylene terephthalate glycol) [3].

Elements manufactured through additive methods exhibit varying mechanical properties [7, 8]. This variability is influenced by factors such as the layer structure, layer height, temperature of the plasticizing nozzle, orientation of the models relative to the prototyping device, and the arrangement

of fibers within each layer [9, 10]. Consequently, these factors are the subject of extensive research. Understanding the mechanical properties of materials is essential for designing elements that can withstand operational loads without undergoing deformation or damage [11, 12].

Rao et al. [8] investigated how the temperature of the plasticizing nozzle affects the tensile strength of PLA samples infused with carbon fibers, examining a range from 205 °C to 225 °C. Their findings indicated that the interactions between layer height and internal structure, as well as nozzle temperature and internal structure, significantly affect the tensile strength. However, no significant interaction was found between layer height and nozzle temperature. Atakok et al. [13] reported that the chosen layer height affects tensile strength by more than 70%. Fontana et al. [14] demonstrated that layer height has a greater impact on mechanical strength than filling density in strength tests of PLA Tough samples. Chacón et al. [15] analyzed the influence of layer height on the tensile and bending strength of PLA samples, finding that the effect of layer height also depends on the model's orientation in relation to the build platform. They also noticed that the plasticity of the samples decreases with the increasing layer height of the printed samples.

The orientation of samples concerning the build platform plays a crucial role in the strength of printed parts. Zhao et al. [16] studied this issue using PLA samples in fused deposition modeling (FDM) with varying layer heights. They observed that Young's modulus increases when changing the sample's position from vertical to horizontal relative to the device's working platform. Similar conclusions were drawn by Yao et al. [17]. Doshi et al. [18] found that the optimal solution for tensile strength and Young's modulus involves placing models flat on the working platform and using full filling.

Additive technologies in cooperation with computer-aided design systems (CAD) enable the design and production of complex structures that are often challenging to manufacture using conventional methods [3, 19]. These structures can have strength properties comparable to solid materials, frequently achieving significant weight reductions [3]. The weight reduction in models produced with additive technologies can also be attained through the use of various types of internal structures and their respective densities [20]. This characteristic is a common subject of research among many authors. For instance, Dev et al. [21] determined the effect of infill on compressive strength using FDM samples made from ABS. They found that samples with an internal gyroid structure density of 80%, with fibers arranged at a 45° angle, exhibited the highest compressive strength in their testing group. Pernet et al. [22] investigated the impact of different infill types and densities (20%, 40%, 60%, 80%, and 100%) on the compressive strength of PLA samples. Their research concluded that the most effective patterns for creating lightweight structures resistant to unidirectional compressive loads were grid and triangular patterns. Similar studies by Nace et al. [23] using thermoplastic polyurethane (TPU) samples confirmed that both the filling pattern and its density influenced the performance of the tested samples. Bhosale et al. [24] observed that increasing the internal structure density from 80% to 90% over shored up the tensile strength of PLA samples by more than 41%. This strength gain was also associated with an increase in the weight of the samples. Ambati et al. [25] also examined the tensile strength of PLA samples, focusing on the effects of filling patterns (grid, gyroid, and triangular) and densities (60%, 75%, and 90%). Their findings indicated that the grid pattern delivered the highest strength, as its structure aligned well with the direction of the tensile force.

Taking into account the above premises, it was decided to conduct research aimed at determining the influence of the selected polymer material and the density of the internal grid-type structure in the static tensile test of standardized samples made using the FFF method. The tests were carried out using type 1A reference shapes manufactured in accordance with the PN-EN ISO 527-2:2012 standard [26].

RESEARCH METHODOLOGY

Materials

For this study, six polymer materials were selected: two commonly used (ABS (acrylonitrile butadiene styrene) and PLA (polylactic acid)), two composite materials based on ABS: HABS (hard acrylonitrile butadiene styrene), and PC/ABS (acrylonitrile butadiene styrene with polycarbonate), two elastomers: HIPS (high-impact polystyrene), and S&S (strong and soft). Table 1 presents the designations of the individual

samples, taking into account both the material used and the density of the internal grid structure in the produced samples, as well as the temperatures for the plasticizing nozzle and the working platform (heatbed). Additionally, Table 2 presents the mechanical properties of the tested polymer materials obtained from the material cards and websites of the filament manufacturers.

Preparation of research samples

The samples for the tensile tests were prepared in accordance with the PN-EN ISO 527-2:2012 standard [26]. The models were created using a CAD program and exported in the.stl format. The dimensions of the samples are illustrated in Figure 1.

Table 1. Tested materials along with the printing process parameters used

Mark	Material	Density of the internal grid-type structure	Temperature of nozzle / heatbed (°C)
A13	ABS	13%	270 / 90
A15		15%	
A20		20%	
A65		65%	
A80		80%	
A100		full (100%)	
P13	PLA	13%	210 / 50
P15		15%	
P20		20%	
P65		65%	
P80		80%	
P100		full (100%)	
HA13	HABS	13%	240 / 100
HA15		15%	
HA20		20%	
HA65		65%	
HA80		80%	
HA100		full (100%)	
PA13	PC/ABS	13%	260 / 100
PA15		15%	
PA20		20%	
PA65		65%	
PA80		80%	
PA100		full (100%)	
PA100J		full unidirectional	
H13	HIPS	13%	235 / 90
H15		15%	
H20		20%	
H65		65%	
H80		80%	
H100		full (100%)	
S13	S&S	13%	250 / 80
S15		15%	
S20		20%	
S65		65%	
S80		80%	
S100		full (100%)	

Table 2. Mechanical properties of tested polymer materials obtained from manufacturers

Parameter	Material					
	ABS	PLA	HABS	PC/ABS	HIPS	S&S
Density (g/cm^3)	1.04	1.24	1.05–1.15	No data	No data	No data
Tensile strength (MPa)	50.99	53	44.13	No data	No data	No data
Flexural strength (MPa)	78.45	83	No data	No data	No data	No data
Elongation at break (%)	30	6	To 60	No data	No data	No data
Young's modulus (MPa)	2216.3	No data	No data	No data	No data	No data

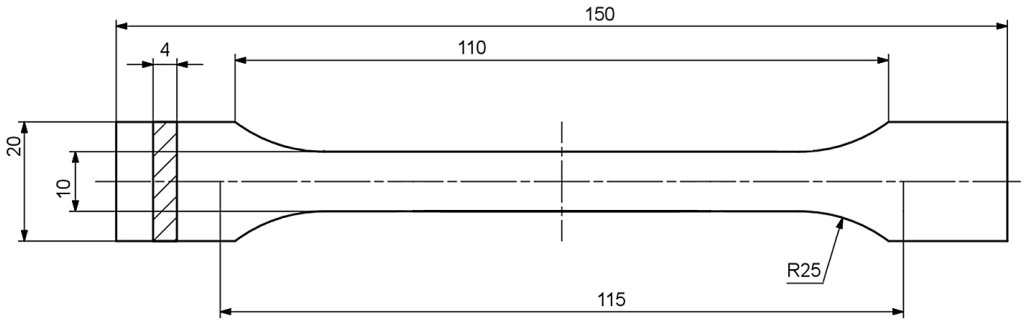

Figure 1. Dimensions of the tensile test sample according to the PN-ISO 527-2:2012 standard [26]

The research used six polymer materials as shown in Table 1. Various internal grid structure densities were applied to the samples: 13%, 15%, 20%, 65%, 80%, and full (100%). The applied densities are shown in Figure 2 on the example of samples made of PC/ABS material. The applied full density with unidirectional fiber arrangement, following with the direction of the given load, included in Figure 2g, was included only in samples made of PC/ABS material due to its properties, which will be discussed later in the article.

For each internal structure density and each polymer material, five samples were produced. The height of each individual layer was set to 0.2 mm, with five complete layers added to the top and bottom of the shape. The samples made from ABS, HABS, HIPS, PC/ABS, and S&S materials were made using the UP BOX+ device (Beijing Tiertime Technology Co. Ltd, Beijing, China), with a closed thermal insulation chamber. In contrast, the PLA samples were created using the Prusa i3 MK3 device (Prusa Research a.s., Prague, Czech Republic) due to the requirement for intensive cooling of individual layers immediately after they were applied. The model support structure (i.e. the structure between the table build platform and the sample being made) was determined as 5 layers. The temperatures for the plasticizing nozzle and build table are presented in Table 1. Figure 3 presents exemplary PC/ABS samples produced on the UP BOX+ device.

STATIC TENSILE TEST

Test parameters

The static tensile test was carried out on an INSTRON 3367 testing machine (Figure 4). The test was divided into individual series, in which samples made of the same material with the same filling density were stretched within one cycle. The sample stretching speed was set to 5 mm/min. During the tests, data on displacement, tensile stresses, and load were recorded.

Performing the test

Figure 5 shows example samples made from the tested materials with an internal structure density of 13% after the strength test.

Tensile test of PC/ABS samples

During the tensile tests of PC/ABS samples (Figure 5e), it was observed that the sample walls aligned with the direction of the tensile load did not break. This indicates that this material has unidirectional high strength. Consequently, it was decided to modify the geometry of samples

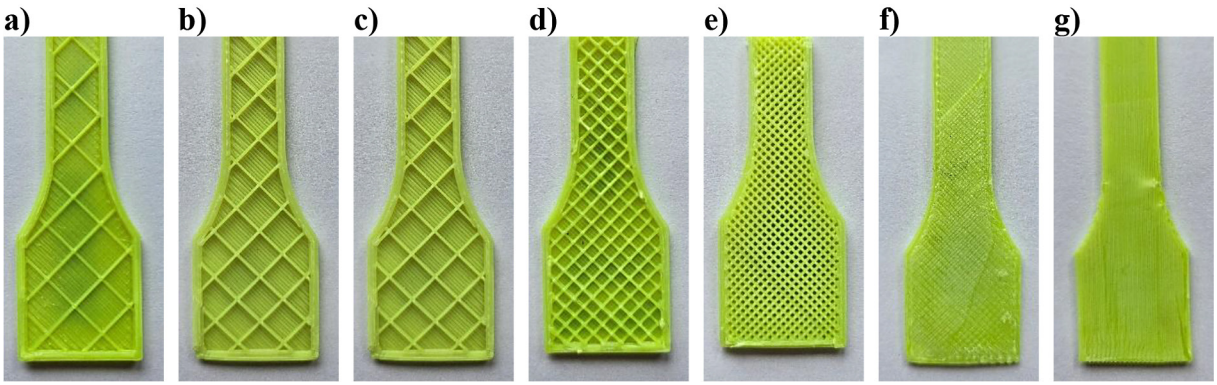

Figure 2. Density of the internal structure on the example of PC/ABS samples: a) 13%, b) 15%, c) 20%, d) 65%, e) 80%, f) full (100%), g) full (100%) unidirectional (only for PC/ABS)

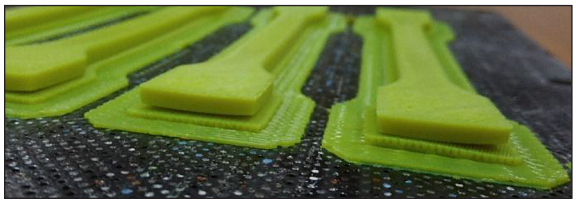

Figure 3. Samples made of PC/ABS material with full density internal structure on the UP BOX+ printer

with full filling density to ensure that individual fibers were oriented along the direction of the load (PA100J – Table 1, Figure 2g). Due to the limited options for changing the printing process parameters in the UP Studio program, which supports the UP BOX+ prototyping device, the model was prepared using Ultimaker CURA 3.6.0 and manufactured on the Prusa i3 MK3 device. The geometry with the fiber arrangement is shown in Figure 6. To ensure similar printing process conditions on the UPBOX+ device, a thermal insulation chamber of comparable volume was constructed and mounted on the Prusa i3 MK3 during the production of PC/ABS samples with the modified geometry.

After making five PA100J samples, they were subjected to a tensile test. An example of the PA100J samples after the strength test is shown in Figure 7. It was noted that despite the modification in fiber orientation, the samples did not completely tear apart. Further testing of samples made of PC/ABS material was thus completed.

Tensile test of S&S samples

Subsequently, tests were conducted on samples made from S&S material. Because of the transparency of the S&S material, additional

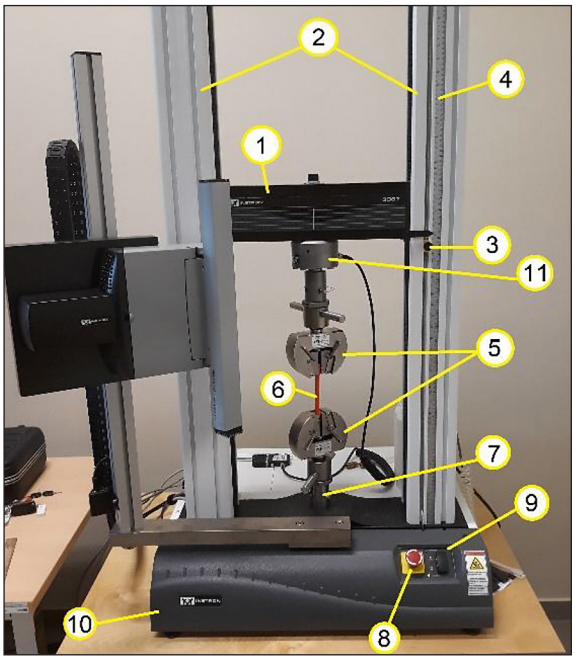

Figure 4. Strength machine INSTRON 3367:
1 – crossbar, 2 – column cover with guide,
3 – lower limiter, 4 – measurement scale,
5 – fit handles, 6 – tested sample, 7 – basic adaptor,
8 – emergency switch, 9 – control panel,
10 – frame base, 11 – load cell

photos were taken of the samples under light to illustrate the flow of material due to the applied load. This phenomenon is shown in selected samples in Figure 8.

By comparing samples S13, S20, and S100 after the tensile test (Figure 8), it was observed that as the density of the internal structure increased, the samples exhibited greater corrugation, narrowings, and increased elongation. Figure 8 also illustrates the changes in the internal structure of the samples as a result of the applied load.

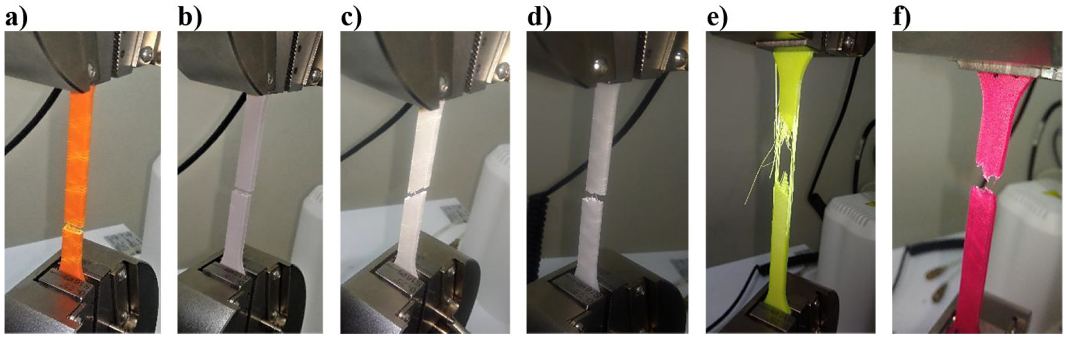

Figure 5. Samples: a) A13, b) P13, c) HA13, d) H13, e) PA13, and f) S13, after tensile test

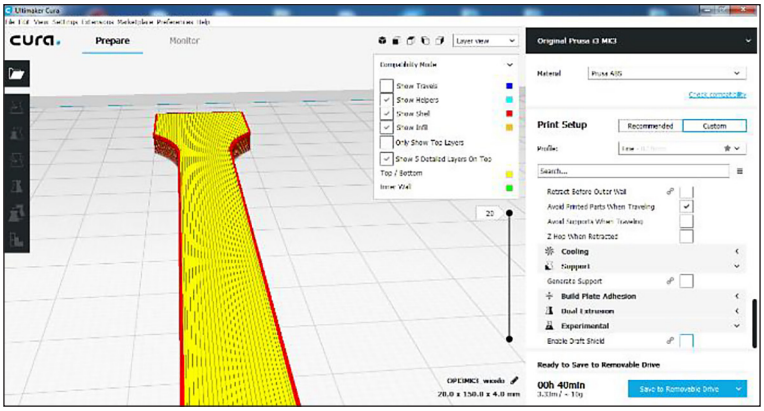

Figure 6. View from Ultimaker Cura showing a sample with changed geometry

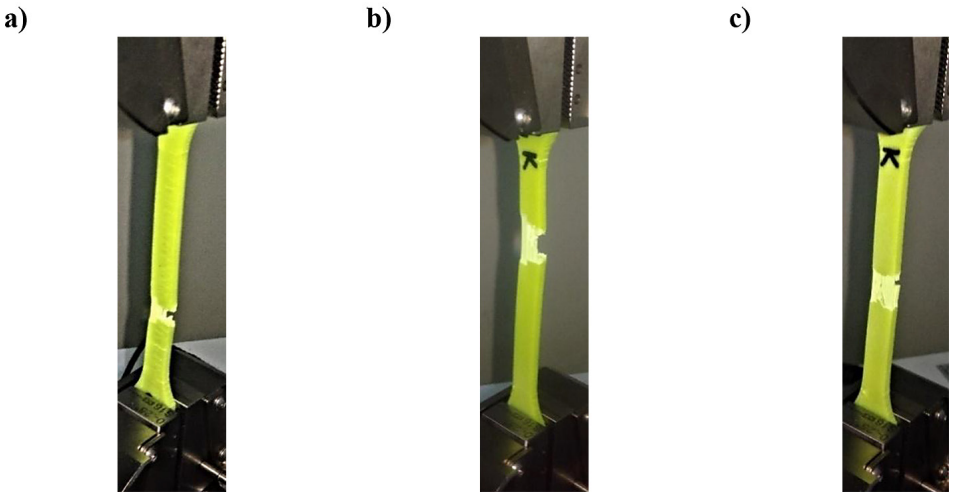

Figure 7. Photographs of selected PA100J samples after the tensile test

Tensile test of HABS samples

During the production of HABS samples, it was noticed that the material was not poured completely into the sample walls (Figure 9). This defect could directly affect the values of tensile stress, load, and displacement measured during the static tensile test.

The underfills (Figure 9) were attributed to the too-low printing speed of the HABS samples. Therefore, a series of tests was conducted, varying the printing speeds in the horizontal plane (XY) of the prototyping device's worktable (ranging from 180 mm/s to 250 mm/s). These tests were executed on a Prusa i3 MK3 device equipped with the previously prepared thermal

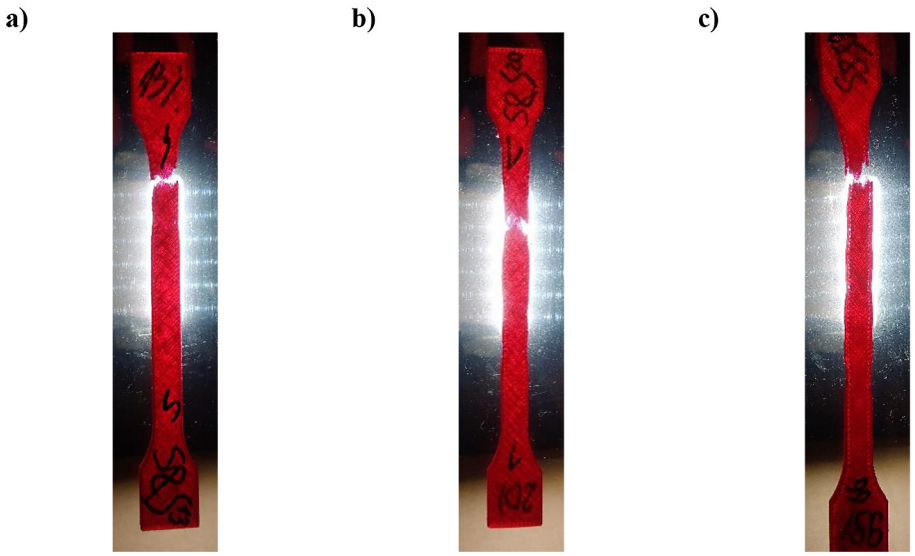

Figure 8. Example of samples: a) S13, b) S20, c) S100, after tensile test

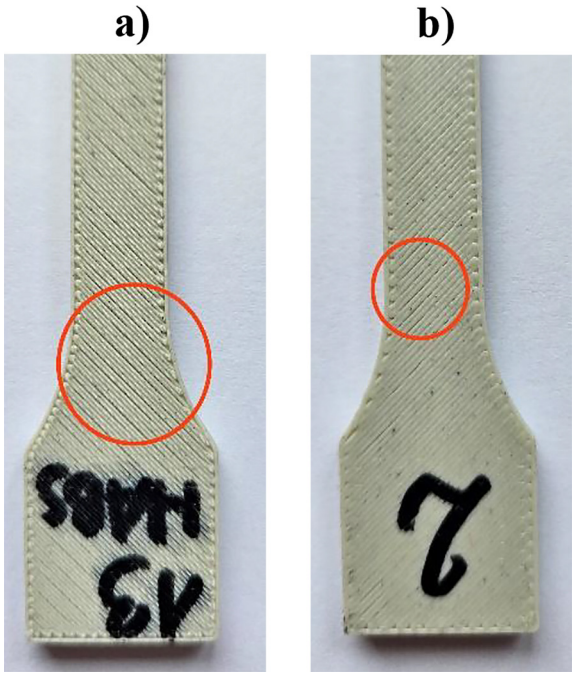

Figure 9. H13 samples in bottom view (a) and top view (b) with marked underfills

insulation chamber to allow for modifications in the software supporting the prototyping device. Attempts to produce the first layers of research samples made from HABS material at different printing speeds are shown in Figure 10.

By comparing the conducted printing tests (Figure 10), it was found that a printing speed of 200 mm/s (Figure 10d) allowed for obtaining the most uniform filling of the HABS material sample. Therefore, the test samples were once again produced using the Prusa i3 MK3 device, this time with the newly selected printing speed of 200 mm/s. These samples were designated based on the example of samples with an internal structure density of 13%: 2HA13.

Performing the test

Following the static tensile test, tensile stress-strain curves were plotted, considering the internal structure densities and materials used. Figures 11–18 showcase example graphs derived from data collected during a series of tests involving five samples with selected internal structure densities from the tested polymer materials. In Figure 11, it is observed that ABS material behaves as a brittle material, exhibiting a distinct yield point. This is consistently observed in other ABS samples with varying internal structure densities.

Similarly, the stress-strain curves for the A13 samples (Figure 11) reflect characteristics akin to those of the P13 samples (Figure 12). The yield point is across all PLA samples tested, followed by a strengthening phase before fracture. The trends for the PLA samples reinforce the notion of plastic-brittle behavior. The same patterns noted in the ABS (Figure11) and PLA (Figure 12) samples are in the HABS samples (Figure 13) regarding yield strength.

To address inconsistencies identified in the HABS samples (Chapter Tensile test of HABS samples, Figure 9), the samples were reprinted at a printing speed of 200 mm/s (Figure 10). The graph for the 2HA100 samples, derived from

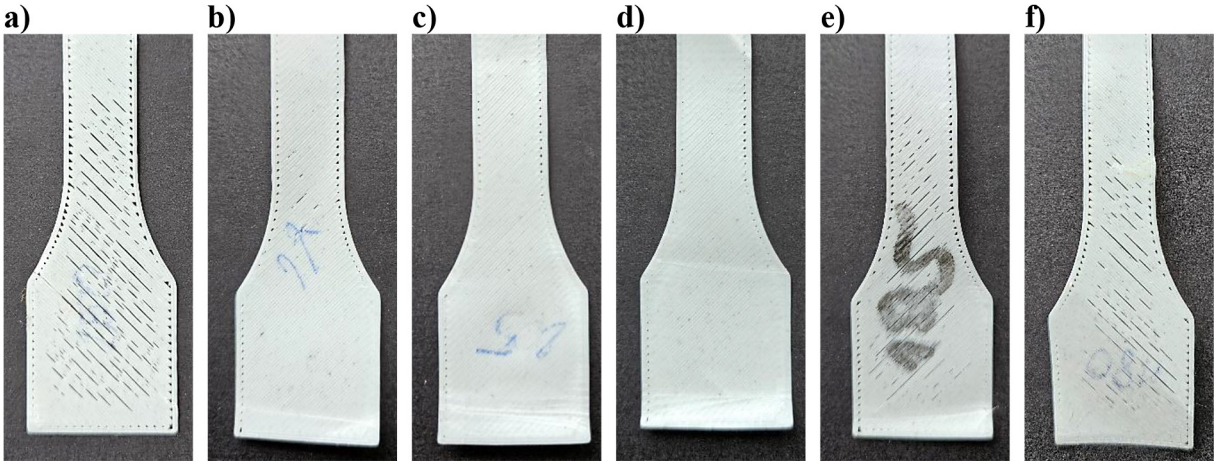

Figure 10. Tests on making samples from HABS material using different printing speeds: a) 250 mm/s, b) 220 mm/s, c) 205 mm/s, d) 200 mm/s, e) 190 mm/s, f) 180 mm/s

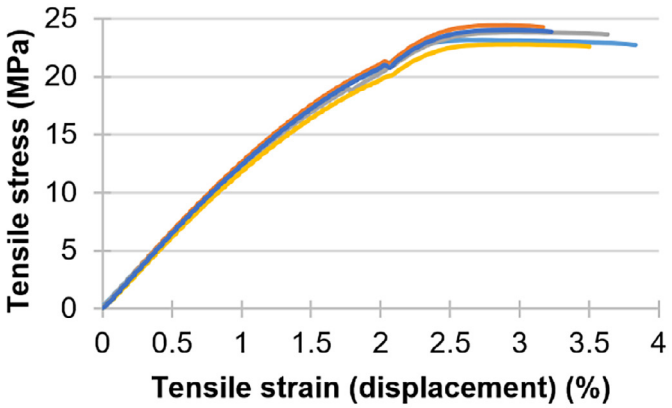

Figure 11. Graph showing the relationship between tensile stress and strain for A13 samples

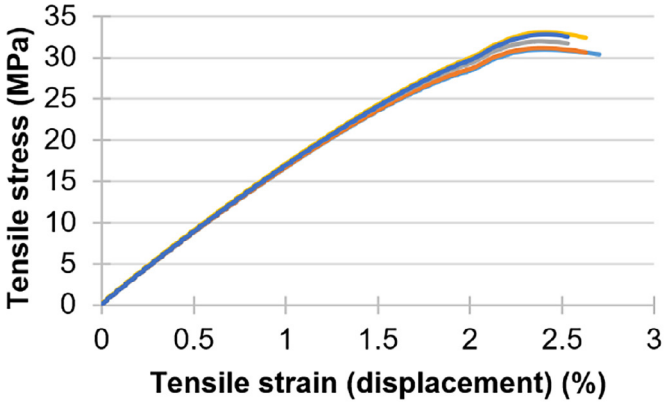

Figure 12. Graph based on data obtained after the tensile test of P13 samples

the tensile test data, is shown in Figure 14. Additionally, the graph for the HA100 samples is shown in Figure 15.

Comparing the tensile tests of HABS samples produced at the default printing speed versus those printed at 200 mm/s, notable differences are observed in samples 2HA100 (Figure 14) and HA100 (Figure 15). In both cases, the graphs indicate materials with a yield point, but the initial gradient for sample 2HA100 (Figure 14) is steeper

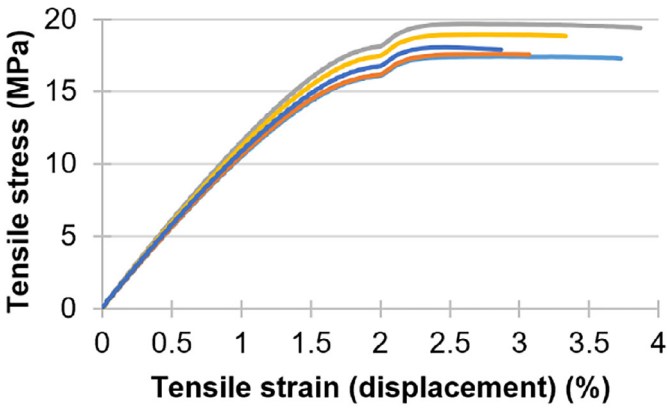

Figure 13. Graph of the curves after the tensile test of HA13 samples

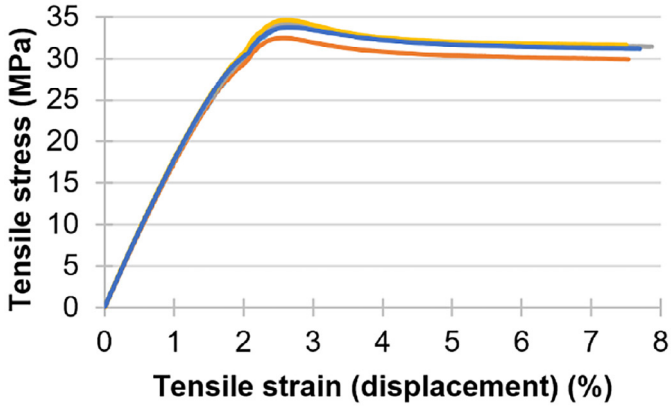

Figure 14. Graph showing the relationship between tensile stress and strain for 2HA100 samples

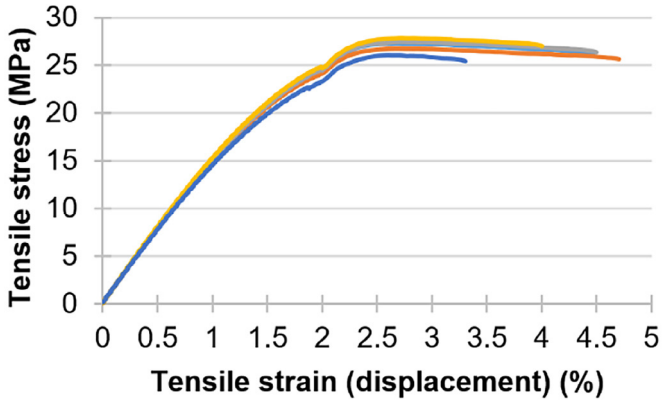

Figure 15. The graph obtained after the tensile test of HA100 samples

as it approaches the yield point. This characteristic reinforces the notion that HABS behaves like a brittle material, in line with the manufacturer's claim that it is a hardened form of ABS.

A similar trend was observed in the tensile test results for all PC/ABS samples (Figure 16), where the yield point was less distinct and the initial graphs displayed steep slopes, further confirming their classification as brittle materials.

In contrast, strength tests conducted on HIPS polymer samples revealed a stepwise change in strain rate (Figure 17). This behavior can be attributed to the two-stage nature of the test, which reflects the properties of the material. In the first

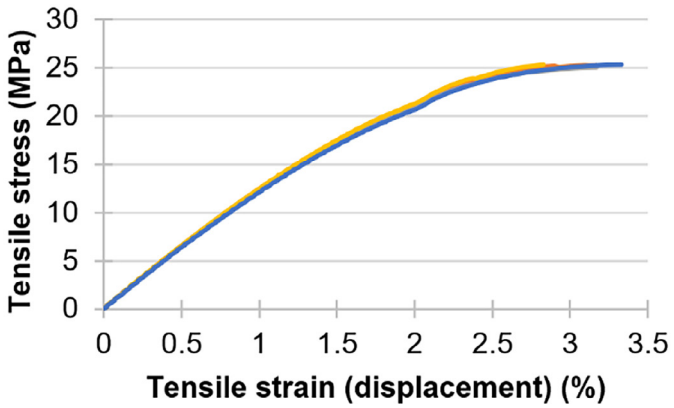

Figure 16. Graph of the curves after the tensile test of PA13 samples

stage, the outer walls were torn, while in the second stage, the central region along with the internal structure failed (Figure 17). Figure 18 illustrates the relationship between tensile stress and tensile strain for the S13 samples.

A comparison of this graph (Figure 18) with those from other polymer materials (Figures 11–17) indicates that the S13 samples also indicate a notable yield point. As the internal structure density increases, the yield point becomes more pronounced, which is accompanied by increased sample elongation. This observation suggests that the S&S material belongs to the category of plastic materials with a high degree of flow.

Development and summary of research results

A static tensile test was carried out on the samples to determine their tensile strength, focusing on the average maximum tensile stress. Table 3 shows the key parameters based on the tested materials and the density of their internal structures after the tensile test. In addition, for samples with complete filling density, the tensile modulus (Young's modulus) was calculated in accordance with the PN-EN ISO 527-1:2020 [27] (Table 4). Notably, the maximum values in both tables are highlighted in red, while the minimum values are marked in blue.

The data presented in Table 4 indicate that the value of Young's modulus is influenced by various factors, including the type of polymer used, the printing speed, and the direction of fiber alignment. To mitigate the issue of underflows (Chapter Tensile test of HABS samples, Figure 9), the printing speed was adjusted to 200 mm/s for samples made from HABS material. This modification resulted in a 16.9% increase in the tensile modulus (an increase of 272 MPa). Additionally, changing the direction of fiber alignment in PA100J samples made of PC/ABS material to align with the applied load direction led to a 29.9% increase in the tensile modulus (by 497 MPa).

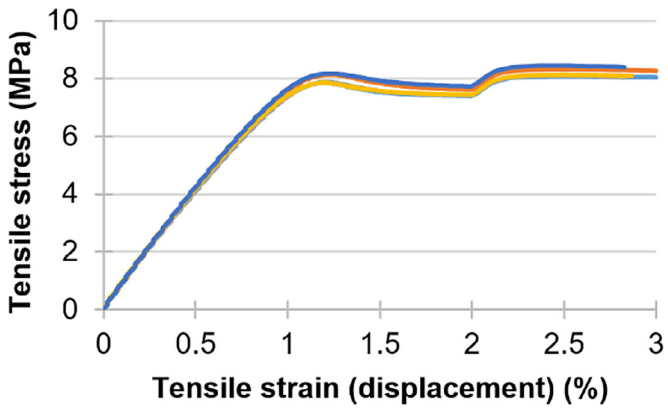

Figure 17. Graph based on data obtained after the tensile test of H13 samples

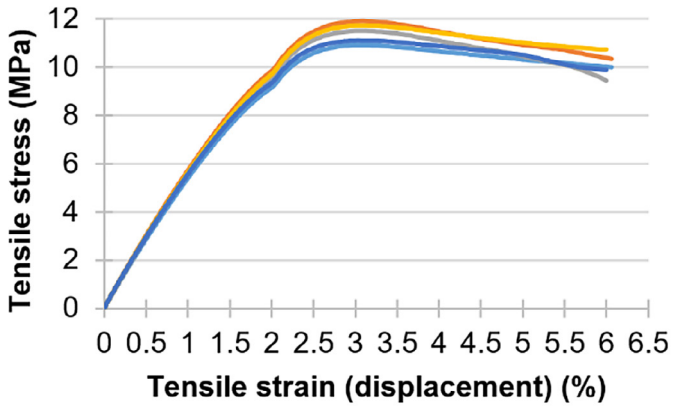

Figure 18. Graph showing the relationship between tensile stress and strain for S13 samples

Furthermore, it is important to compare the tensile modulus values for ABS material provided by the filament manufacturer with the values obtained from the static tensile test (Table 4). The manufacturer's values were based on samples created using injection molding, which typically exhibit greater strength compared to those produced through additive methods.

Based on the obtained data, including tensile strength and displacement at maximum load, graphs were constructed as presented in Figures 19 and 20.

Upon comparing the values for tensile strength (maximum tensile stress) (Table 3, Figure 19) and maximum load (Table 3) from the static tensile tests of samples made from various polymer materials using the FFF method across different internal structure densities, it was observed a consistent trend. Within a single material, tensile strength remained relatively stable across the internal structure density range of 13–65%. For samples made from HIPS material, the parameter values are very similar across all considered densities. A similar trend was noted for HABS and S&S materials in the 13–80% filling density range. Conversely, samples made from ABS, PLA, and PC/ABS materials at 80% and full density exhibit significantly higher values in tensile strength and maximum load compared to those with varying filling densities. The greatest differences were noted between samples made from ABS, PLA, HABS, PC/ABS, and S&S materials when comparing filling densities of 80% and full (100%).

Moreover, a comparison of the tensile strain at tensile strength (Table 3, Figure 20) and displacement at maximum load (Table 3) revealed that in all tested samples made of polymer materials ABS, PLA, PC/ABS, HIPS, and S&S, these values are close to each other, with a minor difference of about 6%. However, exceptions arise with samples featuring 65% and 80% filling density made from HABS material at the default printing speed. These variations can be attributed to material underflows occurring between the fill and the outer contour of the samples (Chapter Tensile test of HABS samples, Figure 9).

FRACTURES OF SAMPLES

Fracture images (Figures 21–26) of selected samples were analyzed after static tensile testing using an ASH OMNI microscope (ASH Ireland – HQ, Kildare, Ireland) at a magnification of 25x.

The examination of the fracture surfaces of ABS samples with varying internal structure densities (Figure 21) revealed a layered-cellular structure, which was notably independent of the filling density applied. The fractures exhibited characteristics typical of brittle fractures, indicated by the sharp edges of the individual layers present on the surfaces (Figure 21). Additionally, there was no observable separation between layers, reflecting a well-integrated and compact structure.

A similar fracture pattern to that seen in the ABS samples (Figure 21) was also observed in PLA samples (Figure 22). The layered-cellular structure of the individual material layers was observed, regardless of the density of the internal structure. A slight separation of the layers was observed at the fracture site. This phenomenon is most likely related to the plastic deformation of the samples during the static tensile test. The

Table 3. Summary of results (mean value and standard deviation) obtained after static tensile test of the tested samples

Mark (Table 1)	Tensile strength (maximun tensile stress) (MPa)	Tensile strain at tensile strength (%)	Maximum load (N)	Tensile strain at maximum load (mm)
A13	23.64±0.58	2.87±0.13	945.56±23.29	2.87±0.13
A15	23.47±1.03	2.69±0.20	938.71±40.95	2.69±0.20
A20	24.71±0.71	2.73±0.07	988.88±28.25	2.73±0.07
A65	24.98±0.96	2.85±0.07	998.99±38.24	2.85±0.07
A80	27.67±0.69	2.87±0.14	1106.72±13.47	2.87±0.15
A100	34.28±0.71	2.72±0.06	1317.06±28.64	2.72±0.06
P13	32.00±0.83	2.39±0.01	1280.13±33.12	2.39±0.01
P15	33.69±0.92	2.53±0.04	1347.68±36.56	2.53±0.04
P20	33.24±0.72	2.51±0.04	1329.76±28.74	2.51±0.04
P65	37.14±1.25	2.47±0.03	1485.66±49.94	2.47±0.03
P80	42.76±0.59	2.54±0.04	1710.53±23.63	2.54±0.04
P100	49.71±1.80	2.65±0.09	1988.41±71.75	2.65±0.09
HA13	18.34±0.84	2.69±0.15	733.69±33.71	2.69±0.15
HA15	18.75±0.21	2.86±0.21	750.23±8.34	2.86±0.21
HA20	19.50±0.51	2.87±0.09	779.82±20.21	2.87±0.09
HA65	18.50±0.20	3.29±0.34	739.87±7.81	3.29±0.34
HA80	19.74±0.50	3.24±0.21	789.72±20.17	3.24±0.21
HA100	27.08±0.62	2.67±0.04	1083.47±24.90	2.68±0.05
2HA13	20.84±0.17	2.50±0.03	833.59±6.98	2.50±0.03
2HA15	21.89±0.26	2.55±0.02	875.68±10.43	2.56±0.02
2HA20	21.49±0.28	2.54±0.05	859.44±11.30	2.54±0.05
2HA65	24.46±0.30	2.49±0.03	978.37±11.92	2.49±0.04
2HA80	27.46±0.46	2.53±0.02	1098.41±19.40	2.54±0.02
2HA100	33.80±0.73	2.63±0.04	1352.14±29.09	2.63±0.04
PA13	25.21±0.22	3.15±0.24	1008.20±5.80	3.16±0.24
PA15	25.07±1.19	3.19±0.19	1002.72±47.38	3.21±0.19
PA20	22.93±0.44	3.08±0.16	917.18±17.77	3.08±0.16
PA65	24.56±0.79	3.12±0.19	982.25±31.77	3.15±0.19
PA80	27.56±0.89	3.37±0.13	1102.52±35.50	3.39±0.13
PA100	31.73±1.89	3.31±0.12	1269.36±75.21	3.33±0.12
PA100J	46.18±0.50	3.40±0.23	1846.94±19.93	3.42±0.23
H13	8.22±0.15	2.49±0.01	329.02±9.96	2.50±0.01
H15	8.84±0.08	2.40±0.06	353.42±3.21	2.40±0.06
H20	8.22±0.18	2.51±0.10	328.79±6.90	2.51±0.10
H65	9.87±0.06	2.42±0.04	394.79±2.29	2.42±0.04
H80	9.90±0.17	2.52±0.03	395.89±6.64	2.53±0.03
H100	9.98±0.29	2.58±0.06	399.22±11.56	2.59±0.06
S13	11.43±0.38	3.06±0.03	457.20±15.15	3.12±0.02
S15	11.95±0.29	3.19±0.07	478.24±11.75	3.24±0.07
S20	12.52±0.53	3.23±0.09	500.89±21.11	3.29±0.09
S65	12.60±0.47	3.30±0.09	503.85±18.77	3.34±0.09
S80	12.83±0.41	3.29±0.19	513.31 / ±16.54	3.34±0.19
S100	16.57±0.76	3.33±0.10	662.79 / ±30.48	3.36±0.10

Table 4. Summary of the Young's modulus values for samples with full internal structure density made of the tested polymer materials

Material	Tensile modulus (Young's module) (MPa)	Tensile modulus (Young's modulus) according to the manufacturer's material card (MPa)
ABS	1834±17.86	2216.3
PLA	2732±16.23	No data
HABS	1606±23.77	No data
HABS (200 mm/s)	1878±14.65	
PC/ABS	1664±66.11	No data
PC/ABS unidirectional	2161±13.60	
HIPS	1008±16.15	No data
S&S	830±21.95	No data

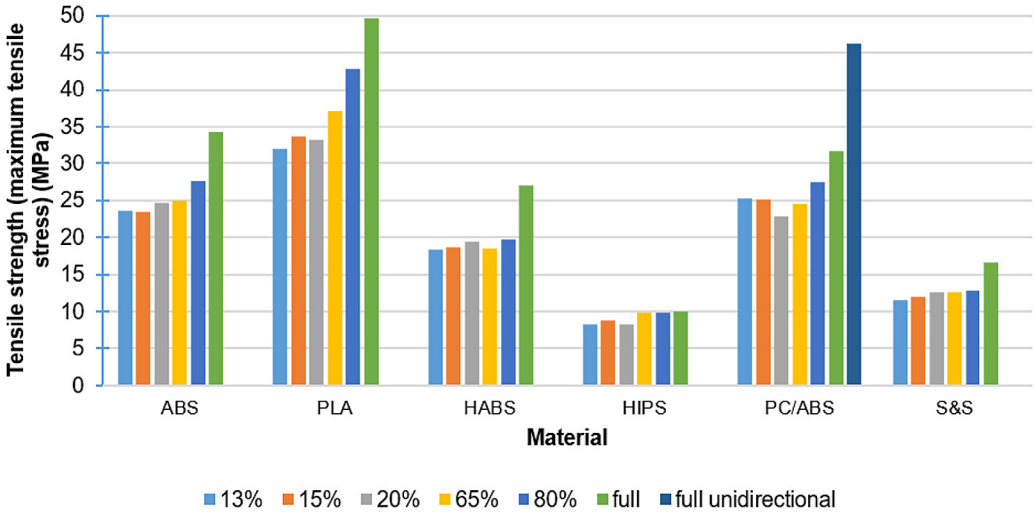

Figure 19. The obtained tensile strength values depending on the density of the internal structure of the samples and the material

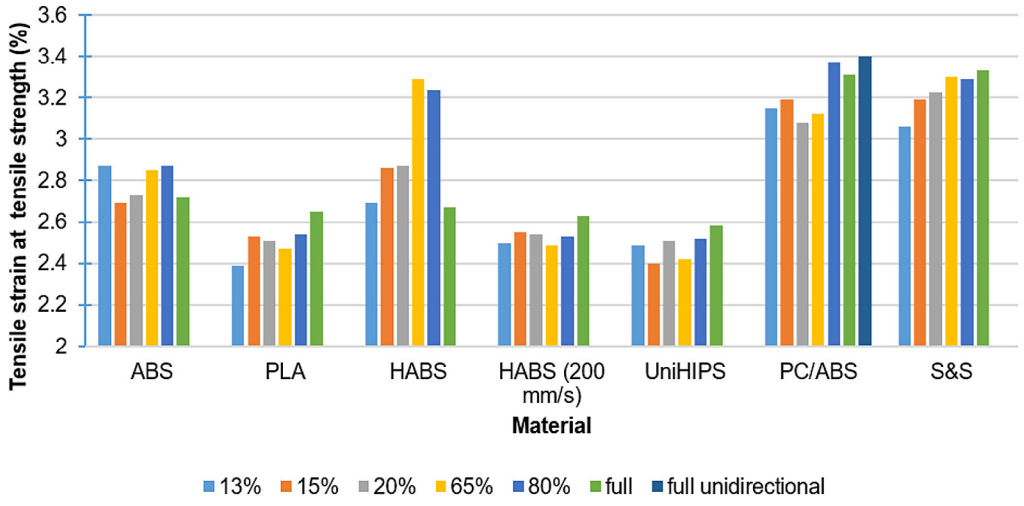

Figure 20. Summary of the obtained values of tensile strain after the tensile test depending on the material and the density of the internal structure

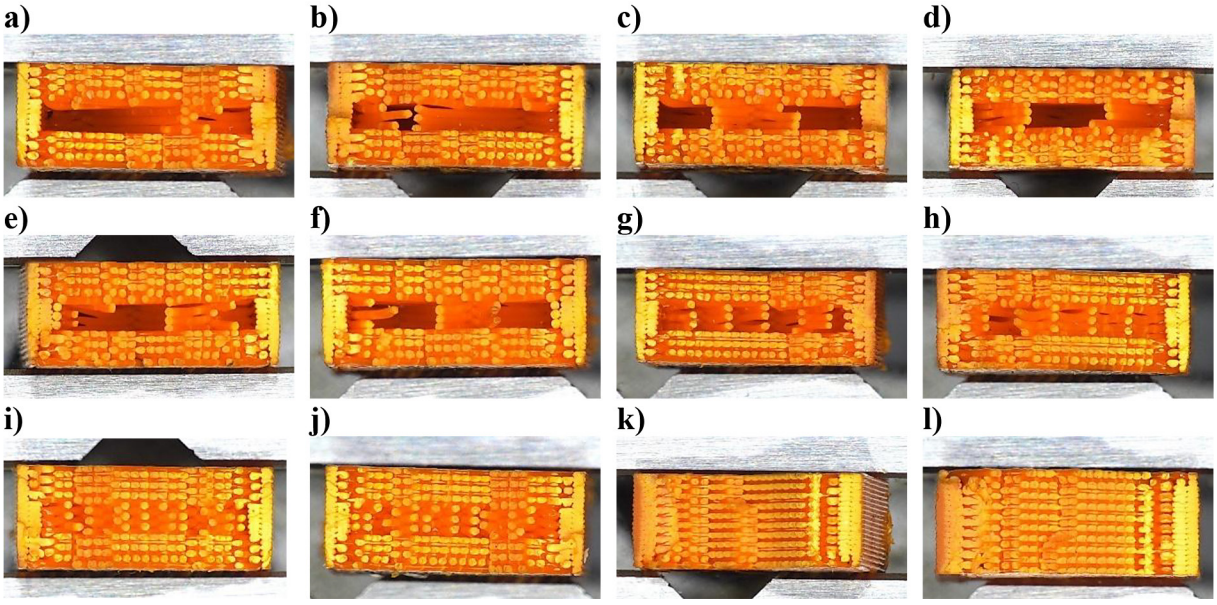

Figure 21. Fracture photos of selected ABS samples after static tensile test taken under a microscope: A13 (a, b), A15 (c, d), A20 (e, f), A65 (g, h), A80 (i, j), A100 (k, l)

absence of visible defects in samples made from PLA material indicates that the softening temperatures of the material (i.e., the temperature of the plasticizing nozzle) and the temperature of the working platform of the prototyping device were well-defined by the manufacturer.

The fracture structure of samples made from HABS material (Figure 23) closely resembled that of the ABS samples (Figure 21), both exhibiting a layered-cellular structure.

Similarly, the layered-cellular fracture structure was observed on the fracture surface of the PC/ABS samples (Figure 24). This was particularly noticeable for sample PA100J (Figure 24m–n), where individual fibers were aligned with the direction of the tensile force. The sharp edges of the fractures, alongside the absence of delamination, indicate that the samples made of PC/ABS material also experienced brittle fractures.

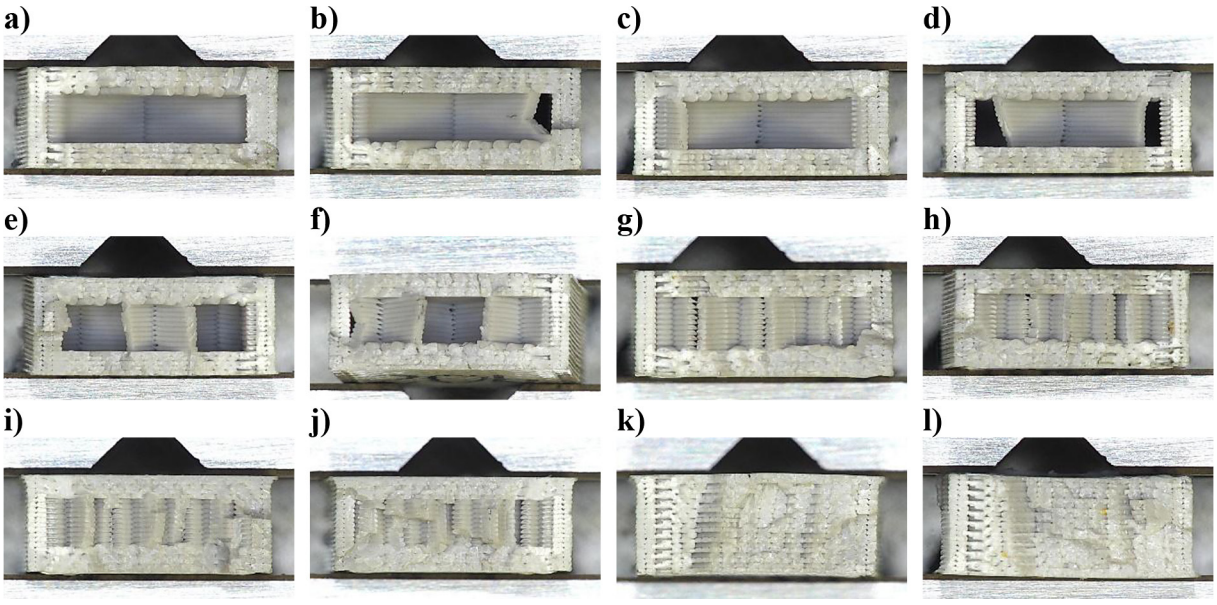

Figure 22. Microscopic views of fractures of PLA samples after static tensile test: P13 (a, b), P15 (c, d), P20 (e, f), P65 (g, h), P80 (i, j), P100 (k, l)

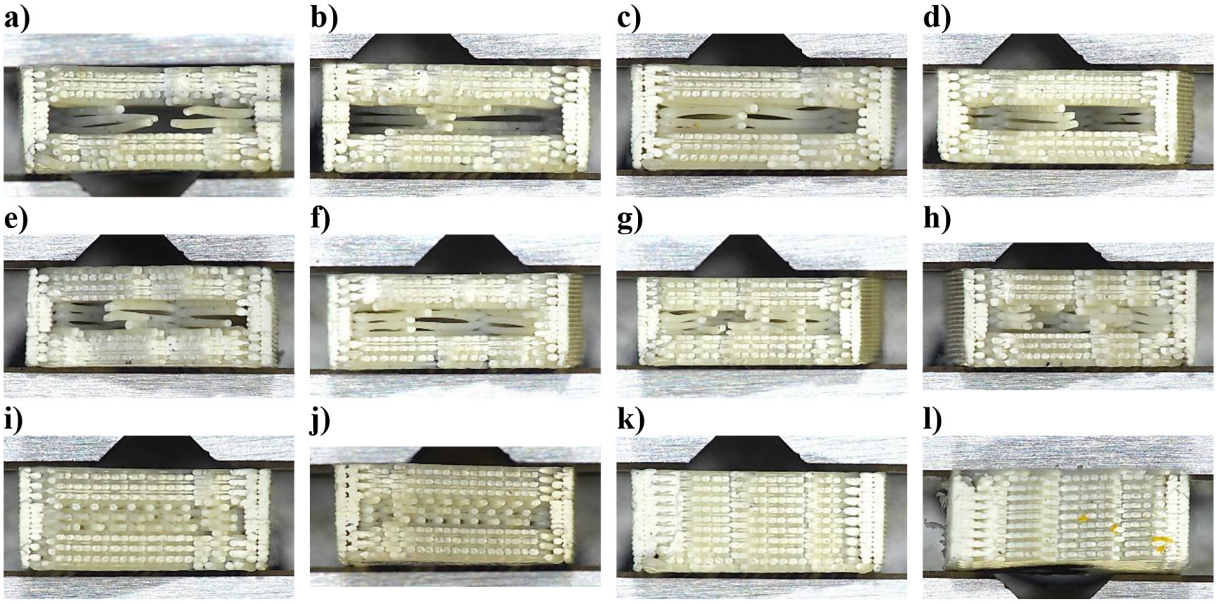

Figure 23. Photos of fractures of HABS samples after strength test: HA13 (a, b), HA15 (c, d), HA20 (e, f), HA65 (g, h), HA80 (i, j), HA100 (k, l)

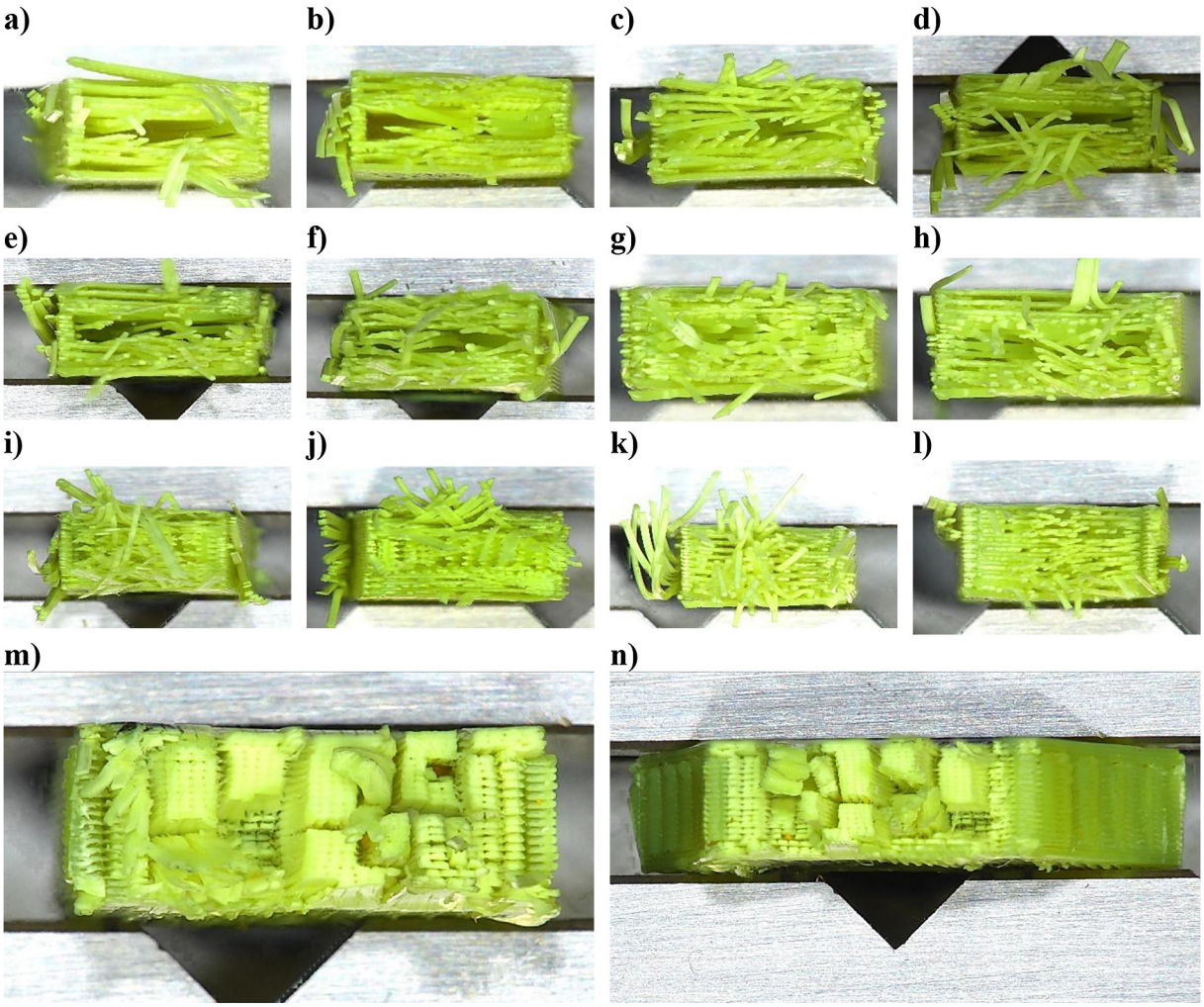

Figure 24. Microscopic pictures of fractures of PC/ABS samples after the static tensile test: PA13 (a, b), PA15 (c, d), PA20 (e, f), PA65 (g, h), PA80 (i, j), PA100 (k, l), PA100J (m, n)

A similar structure observed on the fracture surface of PLA samples (Figure 22) was found in the samples made of HIPS material (Figure 25). A layered-cellular fracture structure of the sharp-edged samples was also observed, with a slight spreading of the individual layers, regardless of the internal structure density used. This observation suggests both brittle and plastic fractures in the HIPS samples. The tensile stress and displacement relationship displayed in the static tensile test graph (Figure 17) supports this, indicating the presence of plastic-brittle fractures in HIPS samples.

In comparison, the fracture photographs of S&S material (Figure 26) showed characteristics typical of ductile fractures, because a significant separation of the layers of the details was observed regardless of the internal structure density. This separation occurred in a plane perpendicular to the direction of the tensile force. It is important to note that the ductile fracture process can be inhibited

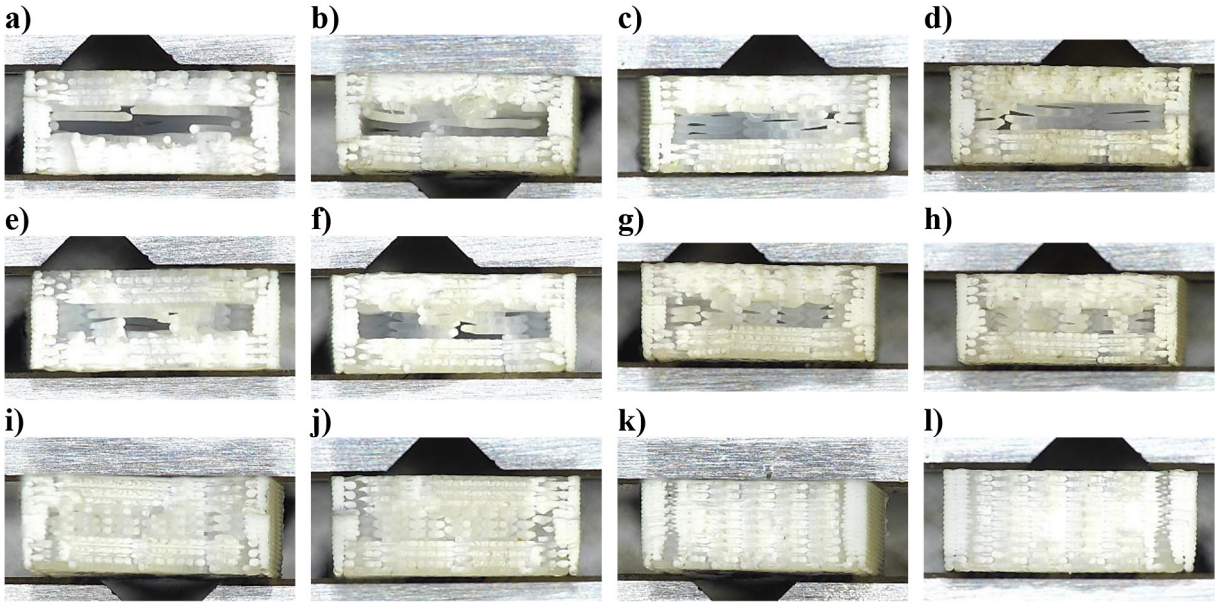

Figure 25. Fracture views of selected HIPS samples after strength test: H13 (a, b), H15 (c, d), H20 (e, f), H65 (g, h), H80 (i, j), H100 (k, l)

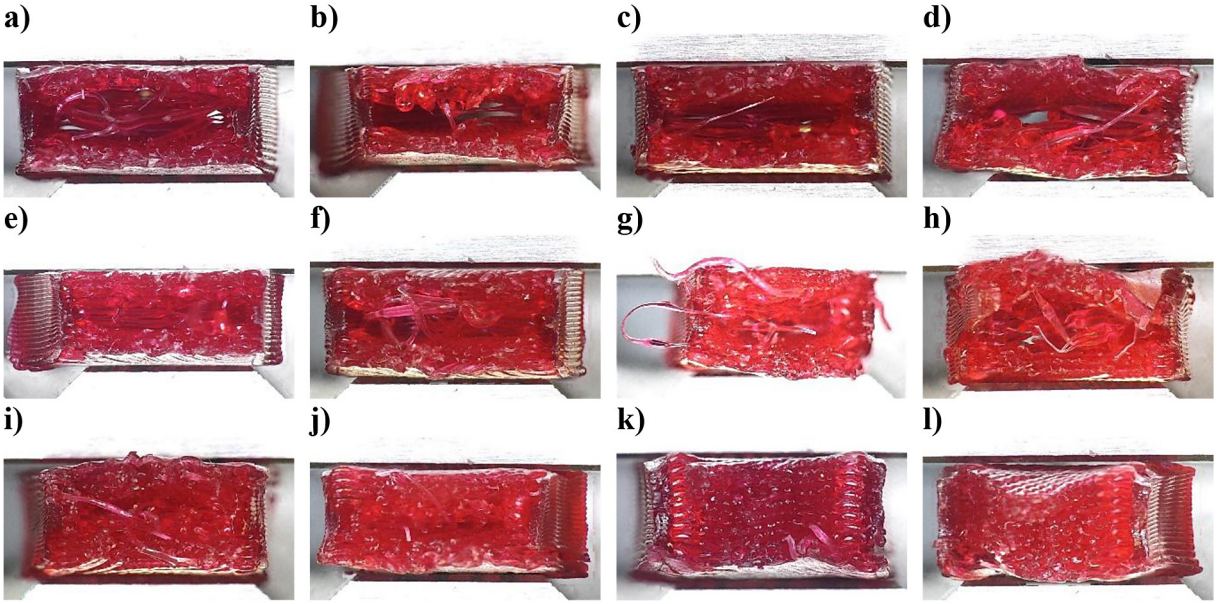

Figure 26. Microscopic photos of fractures of S&S samples taken at 25x magnification after static tensile test: S13 (a, b), S15 (c, d), S20 (e, f), S65 (g, h), S80 (i, j), S100 (k, l)

when tensile stress falls below the yield point of the particular polymer material. Ductile fractures are generally safer than brittle fractures and are less frequent, typically occurring when stress levels approach the material's ultimate strength.

CONCLUSIONS

Samples with an internal structure density ranging from 13% to 65% within a single material had similar values for tensile strength and maximum load. This indicates that it is possible to use lower internal structure density values to achieve strength comparable to that of samples with higher density.

Among all the samples made from ABS, PLA, HABS, PC/ABS, and S&S materials, the most significant differences in tensile strength and maximum load were observed between the samples with an internal structure density of 80% and those that were fully dense.

Variations in results were observed between samples PA100 and PA100J with unidirectional fiber arrangements, contingent on the direction of the applied load. This indicates that in addition to internal structure density, the strength of the models is also significantly influenced by the orientation of individual fibers in relation to the direction of applied force.

In all the tested polymer samples, an increase in internal structure density led to changes in the characteristics of the curves depicting the relationship between tensile stress and load over displacement. As the internal structure density increased, the characteristics of these curves aligned more closely with those that define the general properties of materials outlined in the relevant standards.

The S&S material was marketed by the manufacturer as a high-strength material. However, upon comparing this claim with the obtained results, it became clear that the manufacturer defined the material's strength based on elongation before damage and rupture, rather than specifying its tensile strength, or maximum tensile stress. Additionally, because of the lack of detailed data on the mechanical properties of polymer materials and the common practice of including parameter values from samples produced through injection molding methods, it is necessary to conduct strength tests on polymer materials used in additive methods.

REFERENCES

1. Budzik G., Woźniak J., Przeszłowski Ł. Druk 3D jako element przemysłu przyszłości. Analiza rynku i tendencje rozwoju (in Polish). 1st ed. Rzeszów: Oficyna Wydawnicza Politechniki Rzeszowskiej; 2022.
2. Bulanda K., Oleksy M., Oliwa R., Budzik, G., Przeszłowski Ł., Fal J., Jesionowski T. Polymer composites based on polycarbonate (pc) applied to additive manufacturing using melted and extruded manufacturing (MEM) technology. Polymer 2021; 13. https://doi.org/10.3390/polym13152455
3. Jandal A., Chaturvedi I., Wazir I., Raina A., Haq M.I.U. 3D printing - A review of processes, materials and applications in industry 4.0. Sustainable Operations and Computers 2022; 3: 33–42. https://doi.org/10.1016/j.susoc.2021.09.004
4. Khan I. and Kumar N. Fused deposition modeling process parameters influence on the mechanical properties of ASB: A review. Materials Today: Proceedings 2021; 44: 4004–4008. https://doi.org/10.1016/j.matpr.2020.10.202
5. Peng F., Vogt B.D., Cakmak M. Complex flow and temperature history during melt extrusion in material extrusion additive manufacturing. Additive Manufacturing 2018; 22: 197–206. https://doi.org/10.1016/j.addma.2018.05.015
6. Kaygusuz B. and Özerinç S. Improving the ductility of polyactic acid parts produced by fused deposition modeling through polyhydroxyalkanoate additions. Journal of Applied Polymer Science 2019; 136(43). https://doi.org/10.1002/app.48154
7. Budzik G., Wieczorowski M., Oleksy M., Przeszłowski Ł., Paszkiewicz A., Sobolewski B., Woźniak J., Oliwa R. The Place of 3D Printing in the manufacturing and operational process based on the industry 4.0 structure. Tehnički glasnik 2022; 16(2): 252–257. https://doi.org/10.31803/tg-20220412195706
8. Rao V.D.P., Rajiv P., Geethika N. Effect of fused deposition modeling (FDM) process parameters on tensile strength of carbon fibre PLA. Materials Today: Proceedings 2019; 18(6); 2012–2018. https://doi.org/10.1016/j.matpr.2019.06.009
9. Duarte F.M., Covas J.A., da Costa, S.F. Predicting the effect of build orientation and process temperatures on the performance of parts made by fused filament fabrication. Rapid Prototyping Journal 2022; 28(4): 704–715. https://doi.org/10.1108/RPJ-04-2021-0084
10. Mantecón R., Rufo-Martín C., Castellanos R., Diaz-Alvarez J. Experimental assessment of thermal gradients and layout effects on the mechanical performance of components manufactured by fused deposition modeling. Rapid Prototyping Journal 2022; 28(8); 1598–1608. https://doi.org/10.1108/RPJ-12-2021-0329

11. Dębski M., Magniszewski M., Bernaczek J., Przeszłowski Ł., Gontarz M., Kiełbicki M. Influence of torsion on the structure of machine elements made of polymeric materials by 3D printing. Polimery 2021; 66(5): 298–303. https://doi.org/10.14314/polimery.2021.5.3
12. Singh P.K., Mausam K., Islam A. Achieving better results for increasing strength and life time of gears in industries using various composite materials. Materials Today: Proceedings 2021; 45; 3068–3074. https://doi.org/10.1016/j.matpr.2020.12.062
13. Atakok G., Kam M., Koc H.B. Tensile, three-point bending and impact strength of 3D printed parts using PLA and recycled PLA filaments: A statistical investigation. Journal of Materials Research and Technology 2022; 18: 1542–1554. https://doi.org/10.1016/j.jmrt.2022.03.013
14. Fontana L., Minetola P., Iuliano L., Rifuggiato S., Khandpur M.S., Stiuso V. An investigation of the influence of 3d printing parameters on the tesile strength of PLA material. Materials Today: Proceedings 2022; 57(2): 657–663. https://doi.org/10.1016/j.matpr.2022.02.078
15. Chacón J.M., Caminero M.A., García-Plaza E., Núñez P.J. Additive manufacturing of PLA structures using fused deposition modeling: Effect of process parameters on mechanical properties and their optimal selection. Materials & Design 2017; 124: 143–157. http://dx.doi.org/10.1016/j.matdes.2017.03.065
16. Zhao Y., Chen Y., Zhou Y. Novel mechanical models of tensile strength and elastic property of FDM AM PLA materials: Experimental and theoretical analyses. Materials & Design 2019; 181. https://doi.org/10.1016/j.matdes.2019.108089
17. Yao T., Zhang K., Deng Z., Ye J. A novel generalized stress invariant-based strength model for inter-layer failure of FFF 3D printing PLA material. Materials & Design 2020; 193. https://doi.org/10.1016/j.matdes.2020.108799
18. Doshi M., Mahale A., Singh S.K., Deshmukh S. Printing parameters and materials affecting mechanical properties FDM-3D printed Parts: perspective and prospects. Materials Today: Proceedings 2022; 50(5): 2269–2275. https://doi.org/10.1016/j.matpr.2021.10.003
19. Ali M.H., Issayev G., Shehab E., Sarfraz S. A critical review of 3D printing and digital manufacturing in construction engineering. Rapid Prototyping Journal 2022; 28(7): 1312–1324. https://doi.org/10.1108/RPJ-07-2021-0160
20. Lovo J.F.P., Gerlin Neto V., Piedade L.P., Massa R.C., Pintão C.A., Foschini C.R., Fortulan C.A. Mechanical properties assessment of a 3D printed composite under torsional and perpendicular stress. Rapid Prototyping Journal 2023; 29(1): 1–8. https://doi.org/10.1108/RPJ-03-2022-0067
21. Dev S. and Srivastava R. Experimental investigation and optimization of FDM process parameters for material and mechanical strength. Materials Today: Proceeding 2020; 26(2): 1995–1999. https://doi.org/10.1016/j.matpr.2020.02.435
22. Pernet B., Nagel J.K., Zhang H. Compressive Strength Assessment of 3D Printing Infill Patterns. Procedia CIRP 2022; 105: 682–687. https://doi.org/10.1016/j.procir.2022.02.114
23. Nace S.E., Tiernan J., Holland D., Ni Annaidh A. A comparative analysis of the compression characteristic of a thermoplastic polyurethane 3D printed in four infill patterns for comfort applications. Rapid Prototyping Journal 2021; 27(11): 24–36. https://doi.org/10.1108/RPJ-07-2020-0155
24. Bhosale V., Gaikwad P., Dhere S., Sutar C., Raykar S.J. Analysis of process parameters of 3D printing for surface finish, printing time and tensile strength. Materials Today: Proceedings 2022; 59(1): 841–846. https://doi.org/10.1016/j.matpr.2022.01.210
25. Ambati S.S. and Ambatipudi R. Effect of infill density and infill pattern on the mechanical properties of 3D printed PLA parts. Materials Today: Proceedings 2022; 64(1): 804–807. https://doi.org/10.1016/j.matpr.2022.05.312
26. PN-EN ISO 527-2:2012: Plastics – Determination of tensile properties – Part 2: Test conditions for moulding and extrusion plastics, (Accessed: 28.08.2024). https://sklep.pkn.pl/
27. PN-EN ISO 527-1:2020: Plastics – Determination of tensile properties – Part 1: General principles, (Accessed: 28.08.2024). https://sklep.pkn.pl/